Imaging small three-dimensional elastic inclusions by enhanced multiple signal classification method

Rencheng Song,[a)] Xudong Chen, and Yu Zhong

Department of Electrical and Computer Engineering,

National University of Singapore,

117576 Singapore.

(Dated: July 26, 2012)

Abstract

In this paper, an enhanced MUltiple SIgnal Classification (MUSIC) algorithm is introduced to retrieve 3D small elastic inclusions. Firstly, the multi-static response (MSR) matrix is built by two different ways depending on considering the multiple scattering effect or not. The eigenvalue structure of the MSR matrix is analyzed to identify the degenerate case of scatterers. Secondly, the pseudo-spectrum function is built with an optimal test direction on each node, where a balancing technique is employed to ensure the numerical stability. Benefitting from this MUSIC indicator, the degenerate inclusions can be located with a good performance against noise. Numerical simulations show the proposed method has wider applicability, better resolution, and more robust in presence of noise than the standard MUSIC methods.

PACS numbers: 43.60.Pt, 43.20.Gp

I. INTRODUCTION

The detection of scatterer's properties such as shape, location, and characteristic from the measured scattered data is the subject of inverse scattering problems[1,2]. Various imaging methods[3–12] have been proposed in the past decades due to their wide applications in remote sensing, medical diagnosis and nondestructive testing *et al.*. The multiple signal classification (MUSIC) method[8–11,13–17] is one type of qualitative, non-iterative and deterministic method for locating small inclusions. The MUSIC method builds an indicator (also called pseudo-spectrum function) based on multi-static response (MSR) matrix[13,16] (namely the synthetic scattered data), which peaks at the location of inclusions. All the MUSIC methods stated here refer to time-reversal formulation but not the classical covariance-matrix based MUSIC. To locate inclusions of size much smaller than wavelength, the MUSIC is an ideal method since it is fast and has the ability of resolving inclusions the separation of which is less than the well-known diffraction limit.

Most known works of MUSIC method have been done in the area of acoustic (scalar)[9,14,17] and electromagnetic waves[10,11,13,16]. Recently, Ammari *et al.* introduced a full 3D MUSIC algorithm for the first time to locate small elastic targets[15]. In their method, the MSR matrix was derived based on the asymptotic analysis, and a standard MUSIC method was applied to locate a single non-degenerate scatterer. As known, practical elastic scatterers may be degenerate. Namely, either the density or Lamé coefficients[2,15] of a scatterer can be the same as the background medium. The standard MUSIC fails to locate such scatterers.

In this paper, the MUSIC method in Ref.16 which has the ability to deal with degenerate scatterers in electromagnetic wave is extended to locate isotropic elastic scatterers. However, the extension is not straightforward and two factors make it challenging. Firstly, one non-degenerate elastic scatterer corresponds to nine[15] independent singular vectors of the MSR matrix, as opposed to three[16] for electromagnetic scatterer. It means imaging elastic scatterer is more sensitive to noise than the electromagnetic one. Secondly, two kinds

[a)]Electronic address: elesongr@nus.edu.sg

of contrasts, namely the density and Lamé coefficients contrasts, are considered together in elastic scatterers, which may lead to stability issue due to significant difference in their magnitudes[15].

For the above reasons, the proposed MUSIC method builds the pseudo-spectrum function at each test node with an optimal test direction that is obtained from a subset of signal space. It makes our method applicable for degenerate scatterers and robust against noise. A balancing technique on the test matrix (composed by stress matrix and Green's matrix[15]) is introduced to ensure the stability of searching the optimal test direction. The MSR matrix is built by two different ways depending on considering the multiple scattering effect or not. For several well separated scatterers without considering multiple scattering, the MSR matrix is obtained directly as a sum of scattered field individually excited by each small inclusion. For close scatterers, the Foldy-Lax equation[13,21] is employed to build the exact scattering model with multiple scattering between scatterers. Both the two types of synthetic data are tested. Various numerical simulations show advantages of the proposed method over the standard MUSIC methods, e.g., better resolution, more robust against noise and efficient to locate degenerate objects.

II. THE FORWARD SCATTERING MODEL

Let vectors and matrices be denoted by boldface lower-case letters and boldface capital letters, respectively. Consider M three-dimensional spherical inclusions at $\{\mathbf{x}_j\}_{j=1}^M$, which are illuminated by elastic waves from N transmitters located at $\{\mathbf{r}_j\}_{j=1}^N$ in far field. Suppose the receivers are coincident with transmitters. The orientation directions of transmitters and receivers are three dimensional unit vectors $\{\boldsymbol{\tau}_j\}_{j=1}^N$. Two cases are considered in the forward scattering model, namely, well-separated scatterers and close scatterers.

Firstly, for M well-separated elastic scatterers without considering multiple scattering

effect, the MSR matrix $\mathbf{A}$ is easily obtained by the superposition principle[18] as

$$\begin{aligned}\mathbf{A}_{mn} &= \boldsymbol{\tau}_m^{\mathrm{T}} \cdot \mathbf{u}_n^{sc}(\mathbf{r}_m) \\ &= \sum_{j=1}^{M} \{\mathbf{s}_m^{\mathrm{T}}(\mathbf{x}_j) \cdot \mathbf{M}\left(\delta\lambda(\mathbf{x}_j), \delta\mu(\mathbf{x}_j); |D|(\mathbf{x}_j)\right) \cdot \mathbf{s}_n(\mathbf{x}_j) \\ &\quad + (\mathbf{u}_m^{inc})^{\mathrm{T}}(\mathbf{x}_j) \cdot c(\delta\rho(\mathbf{x}_j), \omega)\mathbf{I}_3 \cdot \mathbf{u}_n^{inc}(\mathbf{x}_j)\} \end{aligned} \tag{1}$$

where the element in $\{\cdot\}$ represents the scattered field due to the jth scatterer which is obtained by asymptotic analysis[15,19,20]. Here $\mathbf{u}_n^{sc}(\mathbf{r}_m)$ is the scattered field received at $\mathbf{r}_m$, $\mathbf{s}_n(\mathbf{x}_j)$ is the stress vector at $\mathbf{x}_j$, and $\mathbf{u}_n^{inc}(\mathbf{x}_j)$ is the incident wave at $\mathbf{x}_j$. They are all excited by the nth transmitter located at $\mathbf{r}_n$. The sign T denotes transpose. $\mathbf{M}$ is the Elastic Moment Tensor (EMT)[15,19,20] at the scatterer $\mathbf{x}_j$. $\mathbf{I}_3$ is a 3×3 identity matrix. $\delta\lambda(\mathbf{x}_j), \delta\mu(\mathbf{x}_j)$ and $\delta\rho(\mathbf{x}_j)$ are contrasts of Lamé coefficients and density at $\mathbf{x}_j$. $|D|$ is volume of the sphere. ω is the angular frequency and $c(\delta\rho, \omega) = \omega^2\delta\rho|D|$. Specific expressions of the above symbols can be found in Ref.15.

Eq.(1) can be written in matrix form, namely,

$$\mathbf{A} = \sum_{j=1}^{M} \mathbf{Q}_j \mathbf{D}_j \mathbf{Q}_j^{\mathrm{T}} \tag{2}$$

where $\mathbf{D}_j = \mathrm{diag}(\mathbf{M}_j, c(\delta\rho_j, \omega)\mathbf{I}_3)_{9\times 9}$ and $\mathbf{Q}_j = [\mathbf{S}_j, \mathbf{G}_j]_{N\times 9}$ with

$$\mathbf{S}_j = [\mathbf{s}_1(\mathbf{x}_j), \ldots, \mathbf{s}_N(\mathbf{x}_j)]_{N\times 6}^{\mathrm{T}}, \quad \mathbf{G}_j = [\mathbf{u}_1^{inc}(\mathbf{x}_j), \ldots, \mathbf{u}_N^{inc}(\mathbf{x}_j)]_{N\times 3}^{\mathrm{T}}.$$

Here $\mathbf{Q}_j$ is propagation matrix while $\mathbf{D}_j$ is scattering matrix. If the jth scatterer is degenerate, for example, the contrasts of the Lamé coefficients are zero, the MSR matrix in Eq.(2) is modified to

$$\mathbf{A} = \sum_{k=1,k\neq j}^{M} \mathbf{Q}_k \mathbf{D}_k \mathbf{Q}_k^{\mathrm{T}} + \mathbf{G}_j \cdot c_j(\delta\rho_j, \omega)\mathbf{I}_3 \cdot \mathbf{G}_j^{\mathrm{T}}. \tag{3}$$

Similarly, if the contrast of density is zero, then

$$\mathbf{A} = \sum_{k=1,k\neq j}^{M} \mathbf{Q}_k \mathbf{D}_k \mathbf{Q}_k^{\mathrm{T}} + \mathbf{S}_j \mathbf{M}_j \mathbf{S}_j^{\mathrm{T}}. \tag{4}$$

Secondly, for close scatterers, the multiple scattering between scatterers needs to be considered. The Foldy-Lax equation is employed to derive the scattering model. For simplicity, we only consider the density contrast here. There is

$$\mathbf{u}_n^{tot}(\mathbf{x}_m) = \mathbf{u}_n^{inc}(\mathbf{x}_m) + \sum_{j=1, j\neq m}^{M} \{-c(\delta\rho(\mathbf{x}_j), \omega)\mathbf{G}_b(\mathbf{x}_m, \mathbf{x}_j)\mathbf{u}_n^{tot}(\mathbf{x}_j)\} \tag{5}$$

$$\mathbf{u}_n^{sc}(\mathbf{r}_m) = \sum_{j=1}^{M} \{-c(\delta\rho(\mathbf{x}_j), \omega)\mathbf{G}_b(\mathbf{r}_m, \mathbf{x}_j)\mathbf{u}_n^{tot}(\mathbf{x}_j)\}, \tag{6}$$

where $\mathbf{u}_n^{tot}(\mathbf{x}_m)$ is the total incident field at $\mathbf{x}_m$ excited by the nth transmitter and $\mathbf{G}_b$ is the Green's function in homogeneous background[15].

Similar to Eq. (1), the MSR matrix $\mathbf{A}$ is built with $\mathbf{A}_{mn} = \boldsymbol{\tau}_m^{\mathrm{T}} \cdot \mathbf{u}_n^{sc}(\mathbf{r}_m)$. Based on Eqs. (5) and (6), the MSR matrix is obtained as

$$\mathbf{A} = \mathbf{R} \cdot \boldsymbol{\Lambda} \cdot (\mathbf{I} - \boldsymbol{\Phi} \cdot \boldsymbol{\Lambda})^{-1} \cdot \mathbf{R}^{\mathrm{T}}, \tag{7}$$

where $\mathbf{R} = [\mathbf{G}_1, \mathbf{G}_2, \ldots, \mathbf{G}_M]$, $\boldsymbol{\Phi}(j,k)$ is null for $j = k$ and otherwise $\mathbf{G}_b(\mathbf{x}_j, \mathbf{x}_k)$, $\mathbf{I}$ is the $3M \times 3M$ identity matrix and $\boldsymbol{\Lambda} = -\mathrm{diag}(c(\delta\rho(\mathbf{x}_1), \omega)\mathbf{I}_3, c(\delta\rho(\mathbf{x}_2), \omega)\mathbf{I}_3, \ldots, c(\delta\rho(\mathbf{x}_M), \omega)\mathbf{I}_3)$. The item $(\mathbf{I} - \boldsymbol{\Phi} \cdot \boldsymbol{\Lambda})^{-1}$ in Eq. (7) indicates the multiple scattering effect between scatters. If the multiple scattering can be ignored, namely $\mathbf{u}_n^{tot}(\mathbf{x}_j) \approx \mathbf{u}_n^{inc}(\mathbf{x}_j)$, the Eq. (7) can be simplified to

$$\mathbf{A} = \mathbf{R} \cdot \boldsymbol{\Lambda} \cdot \mathbf{R}^{\mathrm{T}}, \tag{8}$$

which is same as the one in Eq. (2) when only density contrast is considered.

The synthetic scattering data (MSR matrix $\mathbf{A}$) will be generated by the above two different forward models. It is worth mentioning that once the scattered data are measured (or numerically synthesized), the MUSIC method introduced hereafter is independent of the forward model.

III. THE MUSIC ALGORITHM FOR INVERSE SCATTERING

We introduce the MUSIC method here for the most general case where scatterers have both two kinds of contrasts. The particular case that all scatterers have only the density

contrast or Lamé coefficient contrast can be obtained easily from the general one. We know the MUSIC algorithm is formulated based on the following theorem.

Theorem 1. *Suppose the size of MSR matrix* $\mathbf{A}$ *is sufficiently large. Let* $\mathbf{a} \in \mathbb{C}^9 \backslash \{\mathbf{0}\}$, *then*

$$\mathbf{Q}(\mathbf{x}) \cdot \mathbf{a} \in \mathcal{R}(\mathbf{A}) \quad \textit{if and only if} \quad \mathbf{x} \in \{\mathbf{x}_1, \mathbf{x}_2, \ldots, \mathbf{x}_M\},$$

where $\mathcal{R}(\mathbf{A})$ *denotes the range space of* $\mathbf{A}$.

The proof of Theorem 1 is very similar as Refs.15, 16 and is omitted here. The Theorem 1 implies that the matrix $[\mathbf{Q}_1, \mathbf{Q}_2, \ldots, \mathbf{Q}_M]$ are column-wise linear independent. Thus, from Eq. (2), we get

$$\operatorname{rank}(\mathbf{A}) = \sum_{j=1}^{M} \operatorname{rank}(\mathbf{D}_j).$$

If all scatterers are non-degenerate, $\operatorname{rank}(\mathbf{A}) = 9M$. Correspondingly, for degenerate case, $\operatorname{rank}(\mathbf{A}) = 9M - 6$ for $\mathbf{A}$ in Eq.(3) and $9M - 3$ for $\mathbf{A}$ in Eq.(4).

Suppose the singular value decomposition (SVD) of MSR matrix is $\mathbf{A} = \mathbf{U}\mathbf{\Sigma}\mathbf{V}^{\mathrm{H}}$, where H means the conjugate transpose. In a component form, it's $\mathbf{A} \cdot \mathbf{v}_p = \sigma_p \mathbf{u}_p, \quad p = 1, 2, \ldots, N$. As known, the range space of $\mathbf{A}$ is $\mathcal{R}(\mathbf{A}) = \operatorname{span}\{\mathbf{u}_p; \sigma_p > 0\}$ with dimension $K = \sum_{i=1}^{M} \operatorname{rank}(\mathbf{D}_j)$.

As known, the test direction $\mathbf{a}$ can be chosen arbitrarily for non-degenerate scatterers such that $\mathbf{Q}(\mathbf{x}_j) \cdot \mathbf{a} \in \mathcal{R}(\mathbf{A})$. However, this is not true for degenerate ones. In this section we introduce a way to overcome this difficulty. The optimal test direction $\mathbf{a}_{opt}$ is searched on each test node instead of a fixed one. The proposed method is motived by Ref.16 but it needs a special treatment here to ensure the stability.

A. The search for the optimal test direction

Suppose the angle between vector $\mathbf{v}(\mathbf{x}_j, \mathbf{a}) = \mathbf{Q}(\mathbf{x}_j) \cdot \mathbf{a}$ and $\mathcal{R}(\mathbf{A})$ is $\theta(\mathbf{x}_j, \mathbf{a})$. The condition $\mathbf{v}(\mathbf{x}_j, \mathbf{a}) \in \mathcal{R}(\mathbf{A})$ is equivalent to $\theta(\mathbf{x}_j, \mathbf{a}) = 0$. In other words, if $\mathbf{x}$ is not a scatterer position, $\theta(\mathbf{x}, \mathbf{a})$ must be positive for an arbitrary $\mathbf{a}$. The angle $\theta(\mathbf{x}, \mathbf{a})$ changes with different test directions $\mathbf{a}$ at a fixed test node $\mathbf{x}$. We call the test direction $\mathbf{a}$ that achieves a minimal

angle $\theta_{min}(\mathbf{x}, \mathbf{a})$ at $\mathbf{x}$ as the optimal test direction and denote it as $\mathbf{a}_{opt}(\mathbf{x})$. Following a similar analysis as Ref.16, when an optimal test direction $\mathbf{a}_{opt}(\mathbf{x})$ is employed at each test position, the whole range space in Theorem 1 can be replaced by a more stable subspace $\mathbf{U}_L = \text{span}\{\mathbf{u}_1, \mathbf{u}_2, \ldots, \mathbf{u}_L\}$ which is composed by the first L ($L < K$) leading components of $\mathcal{R}(\mathbf{A})$. In summary, there is

Theorem 2. *Suppose the size of MSR matrix* $\mathbf{A}$ *is sufficiently large. There exists* $\mathbf{a}_{opt}(\mathbf{x}) \in \mathbb{C}^9 \backslash \{\mathbf{0}\}$ *such that* $\mathbf{Q}(\mathbf{x}) \cdot \mathbf{a}_{opt}(\mathbf{x}) \in \mathbf{U}_L$ *if and only if* $\mathbf{x} \in \{\mathbf{x}_1, \mathbf{x}_2, \ldots, \mathbf{x}_M\}$, *where* $L = \max_j\{L_j\}$ *with* $L_j = \sum_{i=1, i\neq j}^{M} \text{rank}(\mathbf{D}_j) + 1$.

Theorem 2 is given here without proof which is similar to Ref.16. Here L_j in Theorem 2 is the minimal dimension of $\mathbf{U}_L$ to locate the jth scatterer and L is the minimal dimension of $\mathbf{U}_L$ to locate all of the scatterers. It should be noted that this analysis is only true for noiseless case.

Then from Theorem 2, the optimal test direction $\mathbf{a}_{opt}$ is solved such that the vector $\mathbf{Q}(\mathbf{x}) \cdot \mathbf{a}$ has the smallest angle to the signal subspace $\mathbf{U}_L$. Thus, $\mathbf{a}_{opt}(\mathbf{x})$ satisfies

$$\mathbf{a}_{opt}(\mathbf{x}) = \arg \max_{\mathbf{a}} \frac{\sum_{i=1}^{L} |\mathbf{u}_i^{\mathrm{H}} \cdot \mathbf{Q}(\mathbf{x}) \cdot \mathbf{a}|^2}{|\mathbf{Q}(\mathbf{x}) \cdot \mathbf{a}|^2}, \tag{9}$$

where $|\cdot|$ denotes the Euclidean length of vector. The $\mathbf{a}_{opt}(\mathbf{x})$ in Eq. (9) is obtained as the eigenvector corresponding to the maximum eigenvalue of the matrix $[\mathbf{Q}(\mathbf{x})^{\mathrm{H}} \cdot \mathbf{Q}(\mathbf{x})]^{-1}([\mathbf{U} \cdot \mathbf{Q}(\mathbf{x})]^{\mathrm{H}} \cdot [\mathbf{U} \cdot \mathbf{Q}(\mathbf{x})])$, where $\mathbf{U} = [\mathbf{u}_1, \mathbf{u}_2, \ldots, \mathbf{u}_L]^{\mathrm{H}}$.

We know

$$\mathbf{Q}(\mathbf{x})^{\mathrm{H}} \cdot \mathbf{Q}(\mathbf{x}) = \begin{bmatrix} \mathbf{S}^{\mathrm{H}}(\mathbf{x}) \cdot \mathbf{S}(\mathbf{x}) & \mathbf{S}^{\mathrm{H}}(\mathbf{x}) \cdot \mathbf{G}(\mathbf{x}) \\ \mathbf{G}^{\mathrm{H}}(\mathbf{x}) \cdot \mathbf{S}(\mathbf{x}) & \mathbf{G}^{\mathrm{H}}(\mathbf{x}) \cdot \mathbf{G}(\mathbf{x}) \end{bmatrix}. \tag{10}$$

Theoretically, $\mathbf{Q}(\mathbf{x})^{\mathrm{H}} \cdot \mathbf{Q}(\mathbf{x})$ is invertible. However, the magnitude of components in $\mathbf{S}(\mathbf{x})$ is usually much larger than that of $\mathbf{G}(\mathbf{x})$ because of the significantly large Lamé coefficients of background medium. Consequently, the matrix $\mathbf{Q}(\mathbf{x})^{\mathrm{H}} \cdot \mathbf{Q}(\mathbf{x})$ in Eq.(10) is nearly ill-conditioned and has a numerical rank 6 (namely, the rank of $\mathbf{S}^{\mathrm{H}}(\mathbf{x}) \cdot \mathbf{S}(\mathbf{x})$). It leads to a difficulty to solve $\mathbf{a}_{opt}$ in elastic wave. This can't occur in Ref.16 where only single contrast is considered.

With the purpose of removing the numerical ill-condition of the matrix, a balanced test matrix can be directly obtained as

$$\mathbf{Q}_b(\mathbf{x}) = [1/q \cdot \mathbf{S}(\mathbf{x}), q \cdot \mathbf{G}(\mathbf{x})], \tag{11}$$

where $q = \sqrt{m/n}$ is a balancing coefficient with

$$m = 1/(6N) \sum_{i=1}^{N} \sum_{j=1}^{6} |\mathbf{S}_{i,j}|, \quad n = 1/(3N) \sum_{i=1}^{N} \sum_{j=1}^{3} |\mathbf{G}_{i,j}|.$$

Thus, $\mathbf{a}_{opt}$ is obtained by substituting $\mathbf{Q}_b(\mathbf{x})$ instead of $\mathbf{Q}(\mathbf{x})$ into Eq.(9).

B. The pseudo-spectrum functions in MUSIC imaging method

The MUSIC method is a qualitative method where an indicator peaks at the location of scatterer. In the standard MUSIC[15], the pseudo-spectrum is defined as

$$W_1(\mathbf{x}) = \frac{1}{\sum_{i=K+1}^{N} |\mathbf{u}_i^{\mathrm{H}} \cdot \mathbf{v}(\mathbf{x}, \mathbf{a})|^2}, \tag{12}$$

where $\mathbf{v}(\mathbf{x}, \mathbf{a}) = \mathbf{Q}_b(\mathbf{x}_j) \cdot \mathbf{a}$, $\mathbf{a}$ is an arbitrarily given test direction and $\mathbf{Q}_b$ is the balanced test matrix in Eq. (11).

As indicated above, $\mathbf{v}(\mathbf{x}_j, \mathbf{a}) \equiv \mathbf{Q}_b(\mathbf{x}_j) \cdot \mathbf{a}$ may be out of the range space of $\mathbf{A}$ for some test direction $\mathbf{a}$ if $\mathbf{x}_j$ corresponds to a degenerate scatterer. However, this can be overcome by use of optimal test direction defined in Section III.A. Suppose the orthogonal projection of $\mathbf{v}(\mathbf{x}, \mathbf{a}_{opt}(\mathbf{x}))$ on the signal subspace $\mathbf{U}_L$ is $\mathbf{q}(\mathbf{x}, \mathbf{a}_{opt}(\mathbf{x})) = [\mathbf{u}_1, \mathbf{u}_2, \ldots, \mathbf{u}_L]^{\mathrm{H}} \cdot \mathbf{v}(\mathbf{x}, \mathbf{a}_{opt}(\mathbf{x}))$. By the relation that

$$\cos(\theta_{min}(\mathbf{x})) = \frac{|\mathbf{q}(\mathbf{x}, \mathbf{a}_{opt}(\mathbf{x}))|}{|\mathbf{v}(\mathbf{x}, \mathbf{a})|},$$

the following pseudo-spectrum function is defined

$$W_2(\mathbf{x}) = \frac{1}{1 - \cos^2(\theta_{min}(\mathbf{x}))} \tag{13}$$

which peaks at the scatterer locations.

The enhanced MUSIC $W_2(\mathbf{x})$ has two advantages. First, at every sampling node $\mathbf{x}$, it chooses the optimal test direction $\mathbf{a}_{opt}(\mathbf{x})$ instead of a fixed one as in the standard MUSIC.

This character makes our algorithm be applicable for degenerate scatterers. Second, the test direction is determined within a subset of signal space because L is smaller than K . Since less small singular values and corresponding singular vectors are involved, the proposed method has a higher resolution in presence of noise.

IV. NUMERICAL SIMULATIONS

Numerical simulations are given to illustrate the performance of the introduced MUSIC method. The problem configurations are as follows. The operating frequency is $f = 2$MHz. The parameters of the background medium are $\rho_b = 7.540 \times 10^3 \text{kg/m}^3$, $\mu_b = 7.246 \times 10^{10}$ Pa and $\lambda_b = 1.087 \times 10^{11}$. A coincident 12×12 planar transmitter and receiver array is located on the plane $z = 10\zeta_p$, where ζ_p is the wavelength of P wave in background medium. The array units are centered at $(0, 0, 10)\zeta_p$ and they are uniformly distributed with distance of two neighboring units as $\zeta_p/2$. The orientation $\boldsymbol{\tau}_j (j = 1, 2, \ldots, 144)$ at each array unit is chosen as one of the three constant vectors, $(-1, 0, 0)^{\mathrm{T}}$, $(0, -1, 0)^{\mathrm{T}}$ or $(0, 0, -1)^{\mathrm{T}}$.

Both noise-free and noise-contaminated cases are discussed. We highlight that here the noise refers to only measurement noise rather than the background medium noise. Two examples are studied, one being single scattering model and the other one multiple scattering model.

A. Example 1

Two degenerate scatterers are considered with locations $\mathbf{s}_1 = (-0.5, 0, 0)\zeta_p$ and $\mathbf{s}_2 = (0.5, 0, 0)\zeta_p$, respectively. The first scatterer has only density contrast and the second one has only Lamé coefficients contrast. The first scatterer has parameters as $\rho_1 = 1.180 \times 10^3 \text{kg/m}^3$, $\mu_1 = 7.246 \times 10^{10}$ Pa and $\lambda_1 = 1.087 \times 10^{11}$, while for the second one they are $\rho_2 = 7.540 \times 10^3 \text{kg/m}^3$, $\mu_2 = 1.015 \times 10^{10}$ Pa and $\lambda_2 = 2.835 \times 10^{10}$. The radius of the two spherical scatterers is $a = \zeta_p/30$. The test domain is a square area $[-1, 1]\zeta_p \times [-1, 1]\zeta_p$ on the $z = 0$ plane. If not stated, the orientation $\boldsymbol{\tau}_j (j = 1, 2, \ldots, N)$ at each array unit is chosen as

a fixed vector $(0, 0, -1)^{\mathrm{T}}$. Since the two scatterers are well separated, the synthetic scattering data of Example 1 are obtained by Eq. (2) without considering multiple scattering.

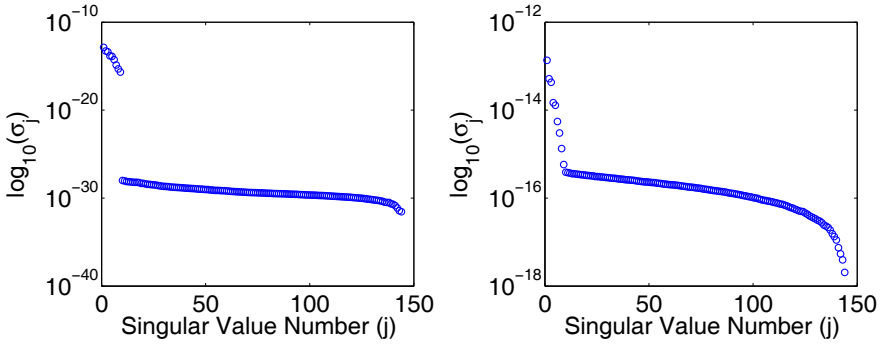

(a) (b)

FIG. 1. (color online) Singular values of the MSR matrix ($j = 1, 2, \ldots, 144$); (a) noise-free case; (b) 30 dB white Gaussian noise contaminated.

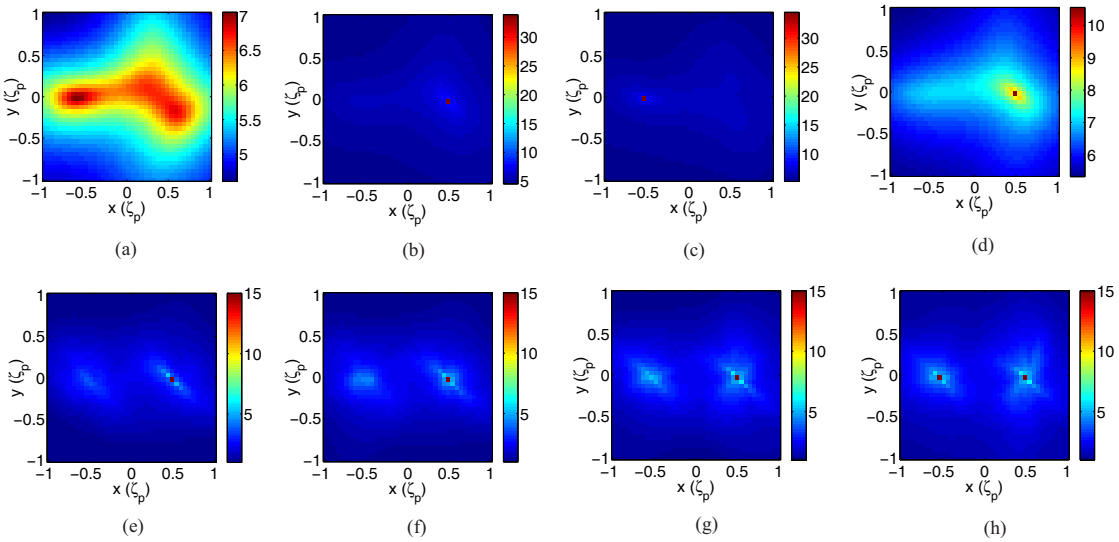

FIG. 2. (color online) The 10-base-logarithm pseudo-spectrums in noise-free case. (a)–(d): pseudo-spectrums of the standard MUSIC algorithm with test directions $\mathbf{a}_1$, $\mathbf{a}_2$, $\mathbf{a}_3$ and $\mathbf{a}_4$, respectively; (e)–(h): pseudo-spectrums of the enhanced MUSIC algorithm with $L = 4, 5, 6$ and 7, respectively.

We first consider the noise-free case. The singular values of the exact MSR matrix

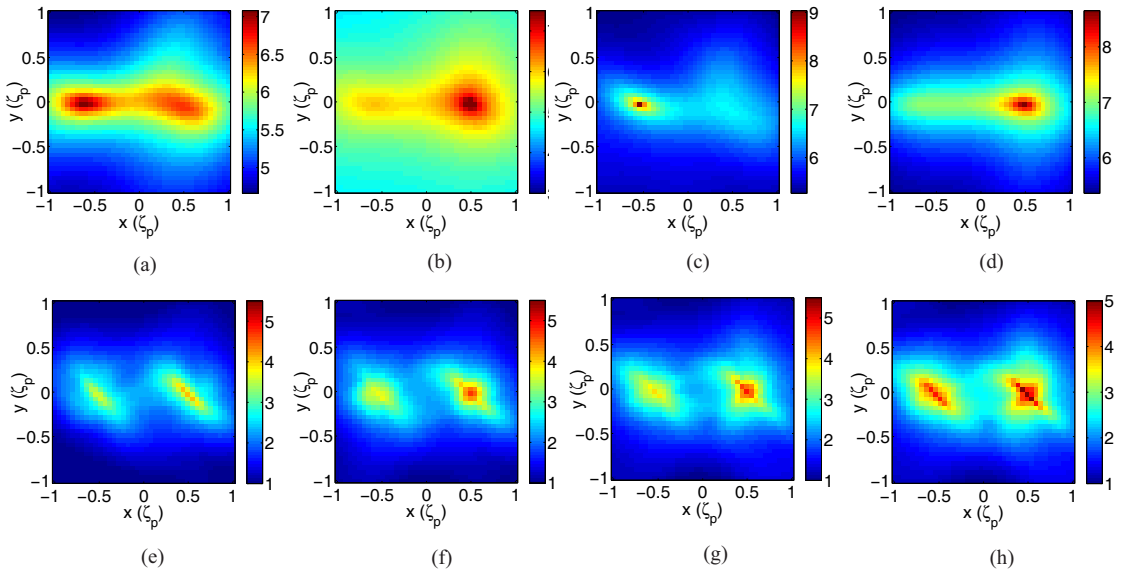

FIG. 3. (color online) The 10-base-logarithm pseudo-spectrums in noise case where 30 dB Gaussian white noise is added to MSR matrix. (a)–(d): pseudo-spectrums of the standard MUSIC algorithm with test directions $\mathbf{a}_1$, $\mathbf{a}_2$, $\mathbf{a}_3$ and $\mathbf{a}_4$ respectively; (e)–(h): pseudo-spectrums of the enhanced MUSIC algorithm with $L = 4, 5, 6$ and 7, respectively.

are shown in Fig. 1(a). We see the first nine singular values are much larger than the others. It means the rank of the MSR matrix is 9 and the signal space is spanned as $\mathcal{R}(\mathbf{A}) = \text{span}\{\mathbf{u}_1, \mathbf{u}_2, \ldots, \mathbf{u}_9\} = \text{span}\{\mathbf{G}(\mathbf{s}_1), \mathbf{S}(\mathbf{s}_2)\}$, where $\{\mathbf{u}_i\}_{i=1}^{9}$ are the first nine singular vectors.

Four 9×1 fixed test directions $\mathbf{a}_1 = (1, 0, 1, 0, 1, 0, 1, 0, 1)^{\mathrm{T}}$, $\mathbf{a}_2 = (1, 1, \ldots, 1, 0, 0, 0)^{\mathrm{T}}$, $\mathbf{a}_3 = (0, 0, \ldots, 0, 1, 1, 1)^{\mathrm{T}}$ and $\mathbf{a}_4 = (1, 0, \ldots, 0, 1)^{\mathrm{T}}$ are tested in the standard MUSIC. Their results are shown in Fig. 2(a)–(d), respectively. We see that at most one scatterer can be imaged with $\mathbf{a}_k, k = 1, 2, 3, 4$. This is because there exists at least one scatterer $\mathbf{s}_j$ such that $\mathbf{Q}(\mathbf{s}_j) \cdot \mathbf{a}_k \notin \mathcal{R}(\mathbf{A})$ for $j = 1, 2$. For example, when $\mathbf{a}_2$ is used, $\mathbf{Q}(\mathbf{s}) \cdot \mathbf{a}_2 \in \mathcal{R}(\mathbf{A})$ is only true when $\mathbf{s} = \mathbf{s}_2$. Thus, only the second scatterer can be imaged with $\mathbf{a}_2$. Similarly, only the first inclusion is imaged with $\mathbf{a}_3$.

Fig. 2(e)-(h) shows the pseudo-spectrums of the proposed enhanced MUSIC with $L = 4, 5, 6$ and 7, respectively. Since $\text{rank}(\mathbf{D}(\mathbf{s}_1)) = 3$ and $\text{rank}(\mathbf{D}(\mathbf{s}_2)) = 6$, from the theoretical

analysis in Section III.A, the minimum L to locate both of the two scatterers is 7. When $L < 7$, only the second scatterer is seen. The numerical results are consistent with the theoretical analysis.

We further consider the noise-contaminated case, where 30 dB measurement additive Gaussian white noise[16] is added to the MSR matrix. The singular values of the noise-contaminated MSR matrix are shown in Fig. 1(b). The singular values corresponding to the noise space are enhanced by noise which makes the boundary between the signal and noise spaces blurred. The pseudo-spectrums of the standard MUSIC method are demonstrated in Fig. 3(a)–(d). The results are similar as those of the noise-free case.

In comparison, Fig. 3(e)–(h) shows the pseudo-spectrums of the enhanced MUSIC method with $L = 4, 5, 6$ and 7 in noise case. Two degenerate scatterers can be seen clearly when $L = 7$. The robustness of enhanced MUSIC method against higher noise is also tested. The orientation $\boldsymbol{\tau}_j (j = 1, 2, \ldots, N)$ at each array unit is chosen randomly from the three fixed directions indicated above. The aim is to increase the information diversity which is important in high-noise case. 20 and 10 dB white Gaussian noises are added to MSR matrix, respectively. The pseudo-spectrums of enhanced MUSIC method with $L = 7$ are shown in Fig. 4. We observe that the enhanced MUSIC method still obtains satisfactory results. It shows our method is robust against noise due to the use of optimal test direction.

B. Example 2

Two degenerate scatterers with only density contrast are considered where their locations are at $\mathbf{s}_1 = (0, 0, 0)\zeta_p$ and $\mathbf{s}_2 = (0.354, 0, 0)\zeta_p$, respectively. Their distance is $0.354\zeta_p$ which is less than half wavelength. The two scatterers have the same parameters as $\rho = 1.180 \times 10^3 \text{kg/m}^3, \mu = 7.246 \times 10^{10}$ Pa and $\lambda = 1.087 \times 10^{11}$. The orientation $\boldsymbol{\tau}_j (j = 1, 2, \ldots, N)$ is chosen randomly from $(-1, 0, 0)^{\mathrm{T}}$, $(0, -1, 0)^{\mathrm{T}}$ or $(0, 0, -1)^{\mathrm{T}}$ at each array unit. Other parameters remain the same as Example 1. Since the two scatterers are close, the synthetic scattering data of Example 2 are obtained from Eq. (7) which considers

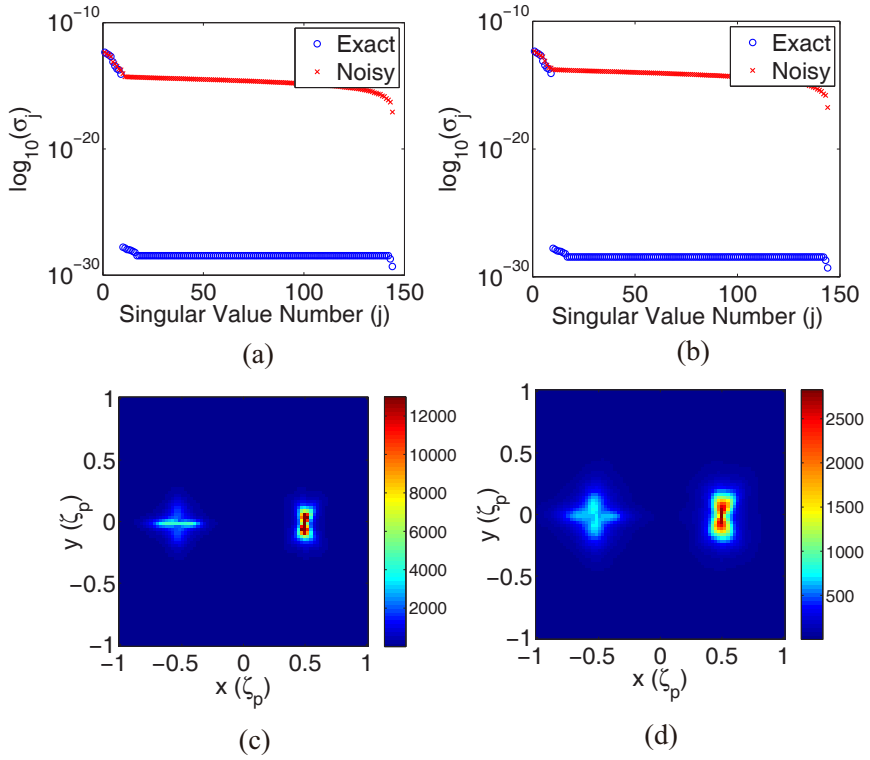

FIG. 4. (color online) Singular values and pseudo-spectrums obtained by the enhanced MUSIC method with different noise levels: (a) The singular values of MSR matrix with 20 dB white Gaussian noise; (b) The singular values of MSR matrix with 10 dB white Gaussian noise; (c) Pseudo-spectrums with 20 dB white Gaussian noise; (d) Pseudo-spectrums with 10 dB white Gaussian noise.

the multiple scattering effect.

Compared to Example 1, the scatterers in this example contains only density contrast. If we don't know this information *a priori*, we have to take the full form MUSIC method. Namely, full test matrix $\mathbf{Q}_b(\mathbf{x})$ in Eq. (11) is employed. Otherwise, if this information is known, the test matrix $\mathbf{Q}_b(\mathbf{x})$ can be reduced to $\mathbf{Q}_b(\mathbf{x}) = \mathbf{G}(\mathbf{x})$. The results of enhanced MUSIC method with both the two kinds of test matrices are shown in Fig. 5 with different noise levels. We observe that utilizing the *a priori* single contrast information achieves better results than the other one. However, both results are satisfactory and super resolution of MUSIC method is observed. We highlight that in high level noise case (10dB for this

example), it's better to make use of as much as possible the known information to achieve a good result. For example, building MSR matrix with more transceivers is helpful in poor SNR (Signal to Noise Ratio) case.

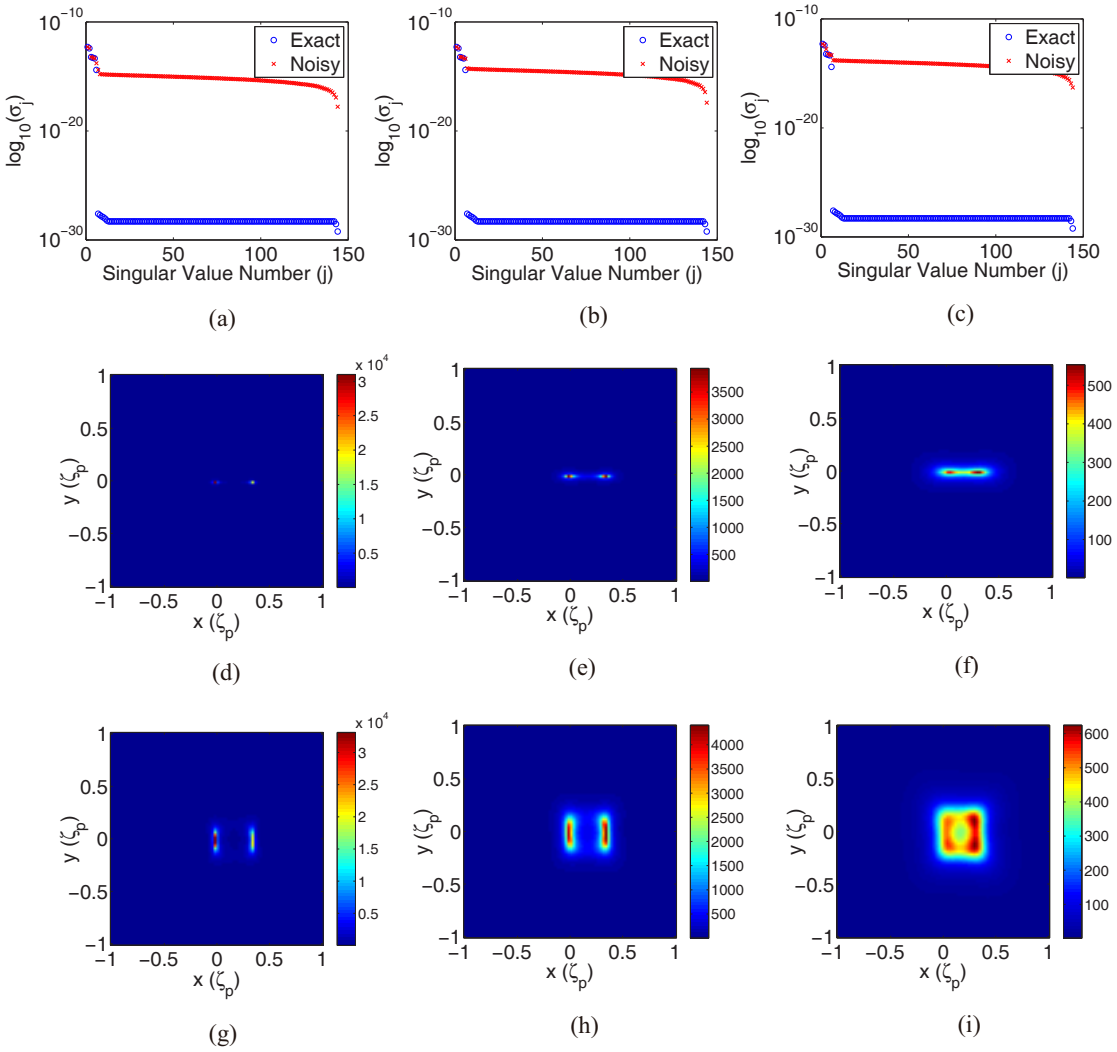

FIG. 5. (color online) Singular values and pseudo-spectrums obtained by the enhanced MUSIC method with different noise levels. From left to right, each column corresponds to 30, 20 and 10 dB white Gaussian noise, respectively. From top to bottom, the first row ((a)–(c)) is singular values of MSR matrix; the second row ((d)–(f)) is pseudo-spectrums of enhanced MUSIC with test matrix $\mathbf{Q}_b(\mathbf{x}) = \mathbf{G}(\mathbf{x})$; the third row ((g)–(i)) is pseudo-spectrums of enhanced MUSIC with full test matrix $\mathbf{Q}_b(\mathbf{x})$ in Eq. (11).

Finally, there are some other concerns to be declared. First, the stability of the MUSIC

method is discussed numerically here. For readers who are interested in theoretical analysis on this issue, please refer to Refs.22–24, where stability and resolution analysis of the standard MUSIC algorithm in the presence of measurement noise have been studied by using random matrix theory.

Second, the computing time of the enhanced MUSIC method is longer than the standard one. As seen above, the MUSIC method is a non-iterative sampling-type method. Its computing time is proportional to the total test nodes. Compared to the standard MUSIC method, an extra 9×9 eigenvalue decomposition needs to be calculated in the enhanced MUSIC method on each node. However, according to our experience, both the two MUSIC methods are very fast if the test nodes are not too many.

Third, here the enhanced MUSIC is only compared with the standard MUSIC method. The comparison with other direct imaging methods such as migration will be our future work and we don't expand this topic here. To our knowledge, in ultrasonic wave, there is already a known work[24] to discuss this issue.

V. CONCLUSIONS

In this paper, the MUSIC method with enhanced resolution has been successfully extended to elastic wave. There are two advantages of our method compared to the standard MUSIC. Firstly, benefitting from the optimal test direction, degenerate scatterers can be located which is usually impossible in the standard MUSIC. Secondly, our algorithm is very robust against noise because only a subset of the signal space is taken to build the indicator. To ensure numerical stability, we have also introduced a special balancing treatment on the test matrix. Two sets of synthetic data are tested, one being single scattering model and the other multiple scattering model. From numerical results, super-resolution is observed. The numerical simulations verify the above good characteristics of the enhanced MUSIC method.

Acknowledgments

This work was supported by the Singapore Temasek Defence Systems Institute under grant TDSI/10-005/1A.

References

[1] D. Colton and R. Kress, *Inverse Acoustic and Electromagnetic Scattering Theory*, 2nd edition (Springer-Verlag, Berlin)(1998), pp. 1–332.

[2] M. Bonnet and A. Constantinescu, "Inverse problems in elasticity", Inverse Probl. **21**, R1–R50 (2005).

[3] D. Colton and A. Kirsch, "A simple method for solving inverse scattering problems in the resonance region", Inverse Probl. **12**, 383–393 (1996).

[4] P. M. van den Berg and R. E. Kleinman, "A contrast source inversion method", Inverse Probl. **13**, 1607–1620 (1997).

[5] T. J. Cui, W. C. Chew, A. Aydiner, and S. Chen, "Inverse scattering of two-dimensional dielectric objects buried in a lossy earth using the distorted Born iterative method", IEEE Trans. Geosci. Remote Sensing **39**, 339 – 346 (2001).

[6] K. Agarwal, L. Chen, N. Chen, and X. Chen, "Multistage inversion algorithm for biological tissue imaging", J. Biomed. Opt. **15**, ID: 016007 (2010).

[7] Y. Zhong and X. Chen, "An FFT twofold subspace-based optimization method for solving electromagnetic inverse scattering problems", IEEE Trans. Antennas Propag. **59**, 914–927 (2011).

[8] A. J. Devaney, "Time reversal imaging of obscured targets from multistatic data", IEEE Trans. Antennas Propag. **53**, 1600–1610 (2005).

[9] A. J. Devaney, E. A. Marengo, and F. K. Gruber, "Time-reversal-based imaging and inverse scattering of multiply scattering point targets", J. Acoust. Soc. Am. **118**, 3129–3138 (2005).

[10] H. Ammari, E. Iakovleva, D. Lesselier, and G. Perruson, "MUSIC-type electromagnetic

imaging of a collection of small three-dimensional bounded inclusions", SIAM J. Sci. Comput. **29**, 674–709 (2007).

[11] E. A. Marengo, R. D. Hernandez, and H. Lev-Ari, "Intensity-only signal-subspace-based imaging", J. Opt. Soc. Am. A **24**, 3619–3635 (2007).

[12] B. E. Anderson, M. Griffa, T. J. Ulrich, and P. A. Johnson, "Time reversal reconstruction of finite sized sources in elastic media", J. Acoust. Soc. Am. **130**, DOI: 10.1121/1.3635378 (2011).

[13] Y. Zhong and X. Chen, "MUSIC imaging and electromagnetic inverse scattering of multiple- scattering small anisotropic spheres", IEEE Trans. Antennas Propag. **55**, 3542–3549 (2007).

[14] X. Chen, "Multiple signal classification method for detecting point-like scatterers embedded in an inhomogeneous background medium", J. Acoust. Soc. Am. **127**, 2392–2397 (2010).

[15] H. Ammari, P. Calmon, and E. Iakovleva, "Direct elastic imaging of a small inclusion", SIAM J. Imaging. Sci. **1**, 169–187 (2008).

[16] X. Chen and Y. Zhong, "MUSIC electromagnetic imaging with enchanced resolution for small inclusions", Inverse Probl. **25**, ID:015008 (2009).

[17] E. G. Asgedom, L. J. Gelius, A. Austeng, S. Holm, and M. Tygel, "Time-reversal multiple signal classification in case of noise: A phase-coherent approach", J. Acoust. Soc. Am. **130**, 2024–2034 (2011).

[18] G. King, *Vibrations and Waves*, 1st edition (John Wiley & Sons, Chichester)(2009), pp. 1–223.

[19] H. Ammari, H. Kang, G. Nakamura, and K. Tanuma, "Complete asymptotic expansions of solutions of the system of elastostatics in the presence of inhomogeneities of small diameter", J. Elast. **67**, 97–129 (2002).

[20] H. Ammari and H. Kang, *Polarization and Moment Tensors: with Applications to Inverse Problems and Effective Medium Theory*, 1st edition (Springer-Verlag, New York)(2007), pp. 1–326.

[21] M. Lax, "Multiple scattering of waves", Reviews Modern Phys. **23**, 287–310 (1951).

[22] H. Ammari, J. Garnier, H. Kang, W. Park, and K. Solna, "Imaging schemes for perfectly conducting cracks", SIAM J. Appl. Math. **71**, 68–91 (2011).

[23] H. Ammari, J. Garnier, and K. Solna, "A statistical approach to target detection and localization in the presence of noise", Waves Random Complex Media **22**, 40–65 (2012).

[24] H. Ammari, J. Garnier, V. Jugnon, and K. Solna, "Direct reconstruction methods in ultrasound imaging of small anomalies", Lect. Notes Math. **2035**, 31–56 (2011).

List of Figures